A Comparison of Two Micromachined Inductors (Bar- and Meander-Type) for Fully Integrated Boost DC/DC Power Converters

Chong H. Ahn, *Member, IEEE*, and Mark G. Allen, *Member, IEEE*

Abstract—**Two micromachined integrated inductors (bar- and meander-type) are realized on a silicon wafer by using modified, IC-compatible, multilevel metallization techniques. Efforts are made to minimize both the coil resistance and the magnetic reluctance by using thick electroplated conductors, cores, and vias. In the bar-type inductor, a 25-μm thick nickel-iron permalloy magnetic core bar is wrapped with 30-μm thick multilevel copper conductor lines. For an inductor size of 4 mm $\times$ 1.0 mm $\times$ 110 μm thickness having 33 turns of multilevel coils, the achieved specific inductance is approximately 30 nH/mm^2 at 1 MHz. In the meander-type inductor, the roles of conductor wire and magnetic core are switched, i.e., a magnetic core is wrapped around a conductor wire. This inductor size is 4 mm $\times$ 1.0 mm $\times$ 130 μm and consists of 30 turns of a 35-μm thick nickel-iron permalloy magnetic core around a 10-μm thick sputtered aluminum conductor lines. A specific inductance of 35 nH/mm^2 is achieved at a frequency of 1 MHz. Using these two inductors, switched dc/dc boost converters are demonstrated in a hybrid fashion. The obtained maximum output voltage is approximately double an input voltage of 3 V at switching frequencies of 300 kHz and a duty cycle of 50% for both inductors, demonstrating the usefulness of these integrated planar inductors.**

I. Introduction

THERE is a large demand for the implementation of a fully integrated switched dc/dc converter on a chip or module. Applications for such converters include distributed power supplies for electronic systems or multichip modules as well as consumer products such as cellular telephones. An additional application area is integrated electrostatic microactuators [1], which usually require a drive voltage of several tens of volts or more (higher than commonly available integrated circuit power supply levels).

Inductive-based switched dc/dc converters are composed of switching control circuits and flyback inductive components. In realizing a dc/dc converter in an integrated fashion, integrated circuits for the switching function are already feasible; however, few planar integrated inductive components that have a sufficient quality factor (Q-factor) to act as a flyback inductor are available. Thus, the major obstacle in realizing an integrated switched dc/dc converter usually comes from the feasibility of planar integrated inductive components [2], [3] with suitable electrical and magnetic characteristics.

In general, it is well known that the volume of magnetic power components for dc/dc switching converters can be reduced as the converter switching frequency is increased. In the conventional magnetic components operating in high frequencies (approximately several MHz), eddy current and hysteresis loss in the magnetic cores rapidly increases as the operating frequency is increased. In addition, conductor coils also have skin depth losses if their thicknesses or diameters are larger than their skin depths at a given frequency. Thus, conventional magnetic components for integrated magnetic power devices at high frequencies are usually limited by these eddy currents and hysteresis losses [4] due to their structures as well as materials used.

In recent years, new micromachining techniques [2], [3], [5] have revolutionized the conventional concept of microstructure fabrication. These micromachining techniques provide several approaches for miniaturization of magnetic power components operated at high frequencies. Cores and conductors of several tens to hundreds of microns in thickness and width with good sidewalls and dimensional control can be easily fabricated. The higher electrical resistance of thin film magnetic cores helps reduce eddy current losses. Skin depth losses at conductors will also decrease when the thickness of thin film conductors is less than their skin depths at a given frequency. At the same time, conductor resistances on the order of several ohms or less is still achievable.

At high frequencies, amorphous alloy and ferrite cores work well as magnetic materials for conventional magnetic components. However, the usual methods of formation of these materials are not compatible with integrated circuit (IC) fabrication processes due to their high processing temperatures (usually higher than 800) as well as the difficulty in patterning these materials using fine-line lithography techniques. In this study, by introducing an electroplated nickel/iron [Ni(81%)/Fe(19%)] permalloy [6] as a magnetic core, low-temperature, CMOS-compatible fabrication is possible. The thin film nature of the core reduces eddy current losses; alternatively, the fabrication technique used is compatible with integrated laminations. In addition, the B-H characteristics of permalloy can also be adjusted by changing the composition of the deposited materials and process conditions [6].

Manuscript received August 8, 1994; revised September 7, 1995. This work was supported in part by the National Science Foundation Grant ECS-9117074.

C. H. Ahn is with the Department of Electrical and Computer Engineering and Computer Science, the University of Cincinnati, Cincinnati, OH 45221 USA.

M. G. Allen is with the School of Electrical and Computer Engineering, Microelectronics Research Center, Georgia Institute of Technology, Atlanta, GA 30332-0269 USA.

Publisher Item Identifier S 0885-8993(96)01935-7.

Thus, hysteresis losses in cores—a major concern in high frequencies—may be controlled.

Prior to implementing a fully integrated dc/dc switched converter, a simple hybrid construction of a switched dc/dc converter using the micromachined inductive components is fabricated to easily assess the feasibility of the integrated inductors. This hybrid prototype uses a bipolar transistor as the switching device and a diode as the complementary synchronized switch. The performance of the converters are compared in terms of the two inductors. Based on this information, fully integrated converters using the inductive components can then be designed.

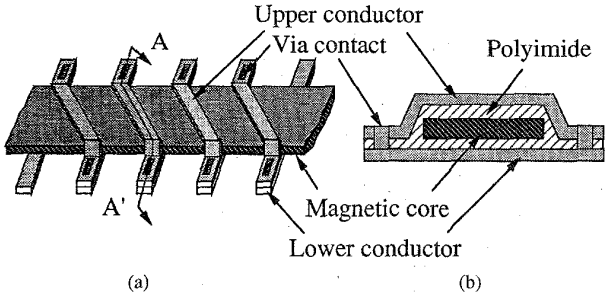

Fig. 1. Schematic diagram of the planar bar-type inductive component: (a) schematic view, (b) A-A′ cut view.

II. Fully Integrated Inductors

Since the fabrication technique of the micromachined inductors presented here is completely different from conventional methods used in the macro scale, feasible geometries in the micro scale are more limited. In addition, fabrication compatibility with integrated circuits is required to maximize the usefulness of the realized inductive components. The typical integrated circuit (IC) fabrication process constrains microstructures to be planar, with patterns made using various types of lithography. Consequently, the general geometries of microstructures feasible in the micro scale should be either two-dimensional (2-D) or quasi-three-dimensional (3-D).

In the macro scale, most conventional toroidal inductors consist of magnetic cores and wrapping wires, which have been manufactured using processes that are incompatible with integrated circuit fabrication techniques. The fabrication of these 3-D inductive structures in a planar geometry has been known to be an extremely difficult task. In previous work done on the planar inductive component used for filters and oscillators [7], [8], the major interest was focused on achieving a high inductance and Q-factor in a planar geometry, without concern over what magnetic flux orientation is favorable. Several geometries of inductive components for magnetic actuator applications have been previously proposed, but none could sufficiently meet the conditions required as magnetic power components. Furthermore, most planar inductive components have been fabricated without using a completely closed magnetic circuit, so that leakage flux from the inductor cannot be neglected, limiting the inductor applications with integrated circuitry.

In this work, two types of inductive components with closed magnetic circuits, the bar-type inductor and the meander-type inductor, are investigated. In particular, emphasis is placed on low-temperature, CMOS-compatible fabrication and high current-carrying capacity of the fabricated inductive component.

A. Planar Integrated Bar-Type Inductor

In the conventional toroidal inductor, conductor wires wrapped around closed magnetic cores result in low leakage flux. Such structures (hereafter referred to as "bar-type" inductors, since the core is in the form of a bar) have been fabricated using multilevel metal schemes to "wrap" a wire around a magnetic core or air core. To demonstrate the feasibility of a planar toroidal inductor, such a component was fabricated by manually wrapping coils around a bar-type magnetic film core in [9]. It was verified from this structure that the introduction of a permalloy thin film increased the inductance value by a factor of 1000 when compared with an air core. However, this device was not fabricated in an integrated fashion.

In this work, microelectronic fabrication techniques are used to fabricate bar-type inductors with high current-carrying capacity [2], [10]. The proposed inductor structure is depicted in Fig. 1. A feature of this inductor is that a closed (i.e., toroidal) magnetic circuit is achieved, minimizing the leakage flux and electromagnetic interference and increasing the inductance value and the Q-factor. The metal interconnections used to construct the wrapping coils usually include metal via contacts. These via contacts are another obstacle in the practical applications of this component since they may have a relatively high contact resistance, which causes a specific heat dissipation in the via contacts. In achieving a high inductance value, if more turns of solenoid coils are required, more via contacts are added, increasing the total coil resistance. Evaporated metal deposition techniques limit the achievable thickness of a deposited metal. In addition, this technique usually causes a high metal contact resistance at the via contacts due to metal oxide or surface contamination resulting from subsequent fabrication processes. As a result, when a high current is applied to the conductor coils, heat is generated locally at the via contacts due to their high resistance, resulting in a potential instability problem in this inductive component.

To solve this problem, in this study, we have used an electroplating technique to fabricate the conductor lines and the vias, because the electroplated metal contacts usually have a low metal contact resistance [11]. If the resistance per via contact can be reduced to several-mΩ range using the electroplating technique, the restriction caused by the high via contact resistance might be removed. Thus, particular efforts have been made to minimize the coil resistance by increasing the thickness of the conductor lines and using electroplated vias.

Fabrication process starts with an oxidized (0.6 μm) 2-in (100) silicon wafer as a substrate. A scanning electron micrograph of the fabricated structure is shown in Fig. 2, which was taken after dry-etching of the polyimide. In the bar-type inductor, a 25-μm thick nickel-iron permalloy magnetic core

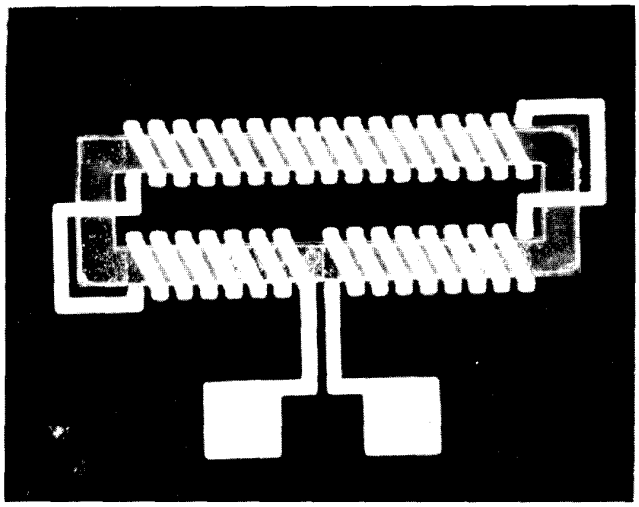

Fig. 2. Photomicrograph of the fabricated bar-type inductor.

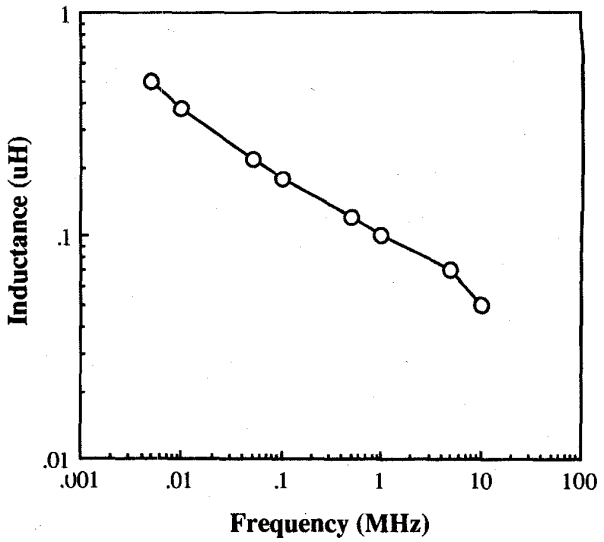

Fig. 3. Measured inductance of the fabricated bar-type inductor as a function of excitation frequency.

is wrapped with 30-μm thick multilevel copper conductor lines, constructing a conventional toroidal inductor in planar shape. For an inductor size of 4 mm $\times$ 1.0 mm $\times$ 110 μm thickness having 33 turns of multilevel coils, the achieved inductance was approximately 30 nH/mm^2 at a frequency of approximately 1 MHz, corresponding to a core permeability of approximately 800. The width of conductor line and bar-core of this inductor are 80 and 300 μm, respectively. The variation of the inductance with frequency is shown in Fig. 3. The measured dc resistance of the conductor line was approximately 0.3 ohms. The stray capacitance of the inductor was derived from the measured impedance and phase as a function of frequency using equivalent circuit analysis. From this analysis, the stray capacitance was shown to be in the several tens of pF region. The effect of the inductance falloff at higher frequencies shown in Fig. 3 is due to both the dependence of the permeability of the iron-nickel core on frequency and the effect of the stray capacitance. The maximum steady dc current that can be achieved in the bar-type is 2.5 A, which gives a maximum allowable current density of 1 $\times$ 10^5 A/cm^2.

B. Planar Integrated Meander-Type Inductor

By interchanging the roles of the conductor and magnetic core in the bar-type inductor, i.e., by wrapping a magnetic core around a planar conductor, an analogous inductive structure can be achieved. A schematic drawing of a section of the integrated toroidal-meander type inductor [12], [13], where toroidal refers to the core geometry and meander refers to the wrapping approach, is shown in Fig. 4. This meander geometry has an advantage over the bar-type geometry in that there are no electrical vias that add resistance to the conductor coil, since the conductor is located in a single plane. A disadvantage of the meander geometry is that the total length of magnetic core (and therefore the core reluctance) is approximately 5% longer than the core length of an analogous bar-type inductor.

The fabrication process also starts with oxidized (0.6 μm) 2-in (100) silicon wafers as a substrate. Fig. 5 shows a scanning

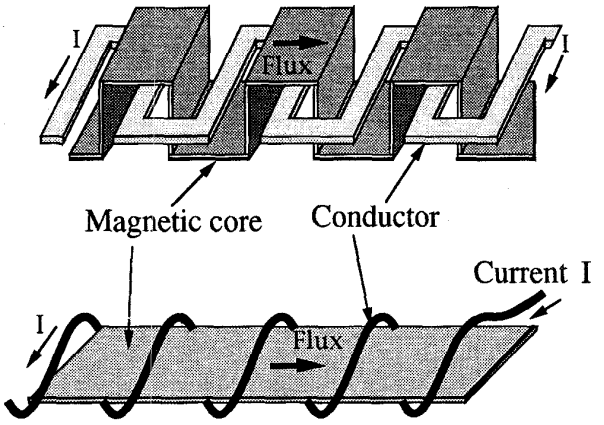

Fig. 4. Schematic diagrams of the integrated meander-type inductor and the more conventional toroidal-type inductor. The structure of the two inductor schemes is analogous: (top) meander-type inductor, (bottom) toroidal-type inductor.

electron micrograph of the fabricated meander-type inductor. The total inductor size is 4 mm $\times$ 1.0 mm $\times$ 130 μm, i.e. the same inductor area as the bar-type; the coil has 30 turns; μ_r is 500; and the cross-sectional areas of the magnetic core and the conductor coil are 300 μm$\times$ 35 μm and 50 μm$\times$ 8 μm, respectively. The magnetic material used was electroplated Ni(81%)-Fe(19%) permalloy [5], and the conductor material used was sputter-deposited aluminum.

The measured inductance values as a function of frequency are plotted in Fig. 6. A fairly flat response through a frequency of 10 MHz (approximately the limit of the impedance analyzer used) is observed. At a frequency of 1 MHz, a specific inductance of 35 nH/mm^2 was achieved.

When this inductor is used as an inductive component for the integrated dc/dc converter, the heat dissipation capability of the inductor will limit the maximum current flowing through the conductors. By applying dc current through the inductor

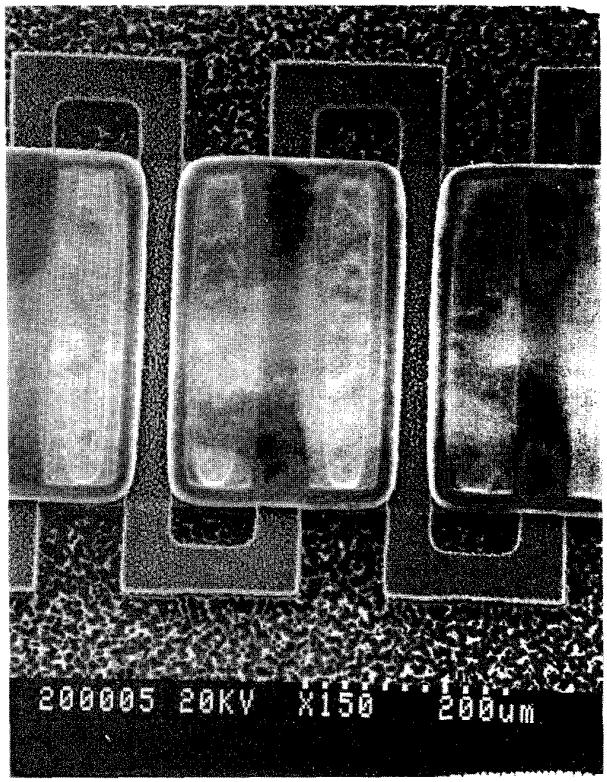

Fig. 5. Scanning electron micrograph of the fabricated meander-type inductor.

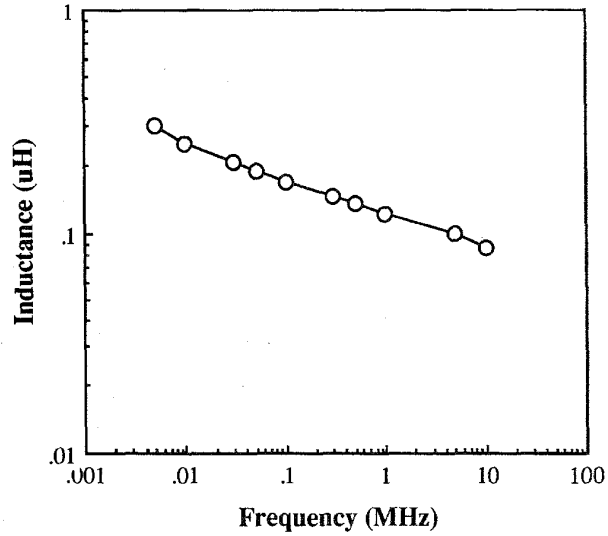

Fig. 6. Measured inductance of the meander-type inductor as a function of frequency.

coils using an Tectronix 370A programmable curve tracer, coil resistance was estimated from the slope of the V-I curve. These results are plotted in Fig. 7. Using the equation of resistance-temperature for the conductor, the temperature of the conductor could be calculated from the measured resistance. This calculation yields a conductor temperature of 50°C at 250 mA. This indicates that the meander film conductor

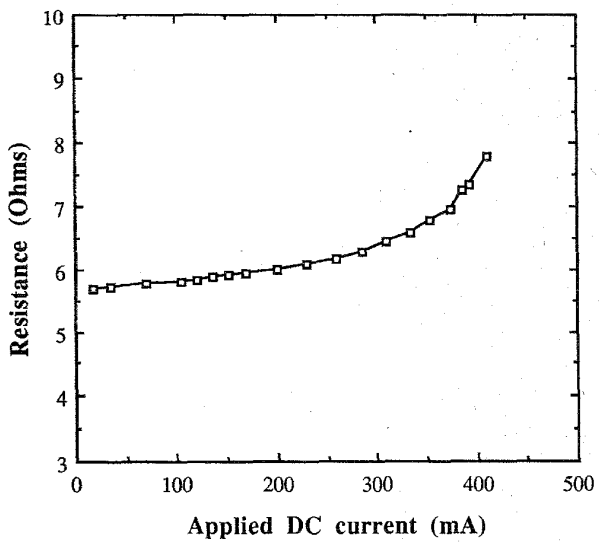

Fig. 7. Resistance of meander conductor from the measured slope of voltage-current curve.

permits high current density. For instance, the maximum recommended current density of conventional inductor [14] in the macro scale at 50°C has been reported as 5×10^2 A/cm^2. In this inductor, it was verified that the attainable maximum current density ranged from 5×10^4 A/cm^2 to 5×10^5 A/cm^2. These values are two orders of magnitude larger than the values in the macro scale, which implies the heat generated from the integrated inductors can be quickly dissipated from the inductors. The total thickness of the inductors is just 130 μm and they are fabricated directly on a silicon wafer, thus the heat generated from the inductors can be easily dissipated through the air and the silicon wafer because most conductors and cores are exposed on or near the surface of the wafer.

The stray capacitance was shown to be in the pF region, and shown to have a negligibly small effect over the frequency ranges used. The effect of the inductance falloff at higher frequencies shown in Fig. 6 is due almost entirely to the dependence of the permeability of the iron-nickel core on frequency as described above.

III. Switched DC/DC Boost Converters

A prototype of a nonisolated, switched dc/dc boost converter [15], which has a single transistor switch configuration, is shown in Fig. 8. The duty ratio D is defined as the ratio of the switch-on time interval to the total switching interval T. In this converter, the output voltage is controlled by regulating the duty ratio of the switching bipolar transistor Q_1.

If the circuit shown in Fig. 8 is idealized by neglecting the internal resistances of the inductor, the transistor, and the diode, the theoretical voltage conversion gain is expressed as

$$\frac{V_0}{V_i} = \frac{1}{1-D}. \tag{1}$$

In the designed dc/dc boost converter, an input voltage of 3 V will be boosted up to 6 V with $D = 0.5$ at approximately

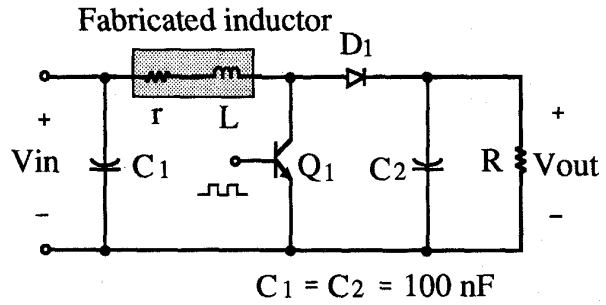

Fig. 8. Circuit diagram of the conventional switched dc/dc boost converter.

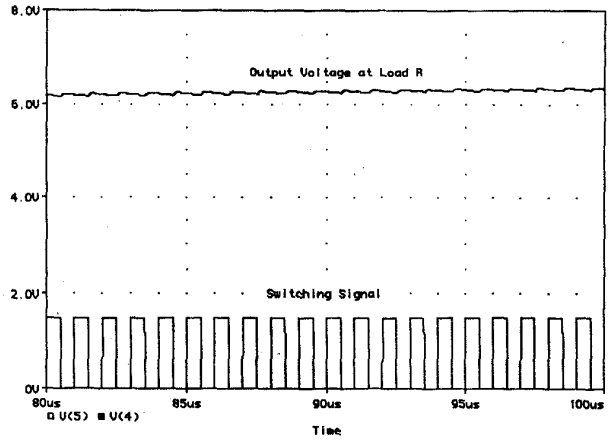

Fig. 9. Simulated output voltage at the load R and at a switching frequency of 1 MHz for $V_{\text{in}} = 3$ V, $r = 1.2$ ohms, $L = 0.542$ μH, $R = 100$ Kohms, $C_1 = C_2 = 100$ nF, and $D = 0.5$.

300 kHz. To choose the values of electrical parameters in the converter, it is assumed that the configurations of the designed converter are as follows: the output power is 40 mW (this power is comparable to the power required to operate an electrostatic microactuator), which requires a maximum output current of 6.7 mA.

To find the parameter values for the rest of the components used in Fig. 8, the dc/dc boost converter is simulated by using the circuit evaluation program Pspice. After choosing different combinations of load impedances, filter capacitors, and internal resistances of inductor, simulations are performed to find appropriate values of these components for subsequent bread-board assembly. Here, the internal resistance and inductance values of the simulated inductor are chosen to approximately match the corresponding values of the fabricated inductors. The simulated output voltage at a switching frequency of 1 MHz is plotted in Fig. 9, where $V_{\text{in}} = 3$ V, $r = 1.2$ ohms, $L = 0.542$ μH, $R = 100$ Kohms, $C_1 = C_2 = 100$ nF, and $D = 0.5$. As shown in Fig. 9, the input voltage of 3 V can be sufficiently boosted to 6 V by using these electrical parameters.

However, the inductor, transistor, and diode shown in Fig. 8 actually include internal resistances denoted as r, r_{ts}, and r_d, respectively. The theoretical voltage conversion gain expressed

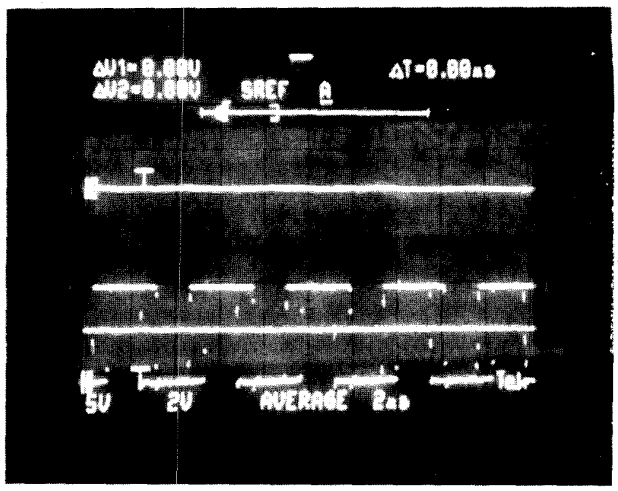

Fig. 10. Waveform of the output voltage of 6 V at the load resistor, where the switching frequency is 300 kHz, the duty cycle is 50%, and the applied input voltage is 3 V.

in (1) is not appropriate in this case. Thus, the voltage conversion gain [16] can be written as

$$V_0 = \frac{V_i - (DV_{Q1} + D'V_D)}{D'} \frac{R}{R + (Dr1 + D'r2)/(D')^2} \quad (2)$$

where $r_1 = r + r_{\text{ts}}, r_2 = r + r_d, D' = 1 - D$, and V_{Q1} and V_D denote the voltage drops at the transistor Q_1 and the diode D_1, respectively.

The load resistance is varied from 5 ohms to 1.2 Mohms, and other electrical parameters are assumed as $r = 1.2$ ohms; $r_{\text{ts}} = r_d = 0.5$ ohms; $V_{Q1} = 0.45$ V; and $V_D = 0.65$ V. As predicted and discussed in [16], an instability arises if the load resistance is less than 20 ohms and then the dc output voltage jumps down to a lower level although the duty ratio increases. However, when the load resistance is much larger than the internal resistance, the output voltage is rapidly increased as the duty ratio increases, as shown to be in Fig. 11.

IV. DC/DC Converter Performance and Discussion

Dc/dc boost converter circuits are then constructed in hybrid fashion using the fabricated inductive component as well as switching components described in Fig. 8. Fig. 10 shows the wave form of the output voltage of 6 V at the load resistor, where the switching frequency is 300 kHz, the duty cycle is 50%, and the applied input voltage is 3 V.

The plot of output voltage variation for the various load resistances is shown in Fig. 11. In both cases, the obtained output voltages for the various load resistance are increased and approach 6 V as the load resistance is increased. The measured and calculated output voltages as a function of duty cycle are plotted for both inductors in Fig. 12, with an input voltage of 3 V. The calculated output voltage is evaluated from (2) using the electrical parameters measured from the meander-type inductor. The measured current flowing through the inductors is proportional to the duty cycle of the converter as shown in Fig. 13. This current reaches approximately 150

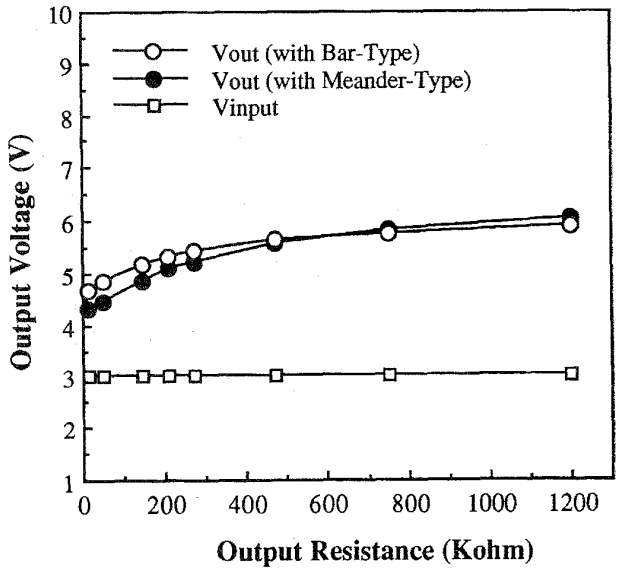

Fig. 11. Output voltage variation for the various load resistances, where the switching frequency is 300 kHz, the duty cycle is 50%, and the input voltage is 3 V.

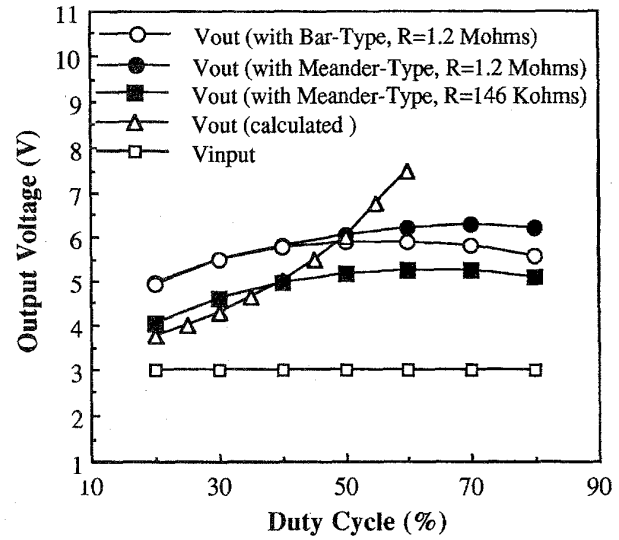

Fig. 12. Measured and calculated output voltages as the function of duty cycle at the input voltage of 3 V, where the calculated values are evaluated from (2) with the meander-type inductor.

mA at a duty cycle of 50% in the bar-type and the duty cycle of 70% in the meander-type inductor. From the core geometries and the B-H characteristics of both inductors, inductor currents of 150 mA in the bar-type inductor and 180 mA in the meander-type inductor produce a flux density of 0.8 Tesla in the inductor cores.

Based on these currents for the magnetic flux saturation, the sensible current density for the appropriate operation of the dc/dc converter have to be less than approximately 2×10^4 A/cm^2, although the attainable maximum current density is ranged from 5×10^4 to 5×10^5 A/cm^2 as described earlier. The efficiency of the dc/dc converter achieved using the

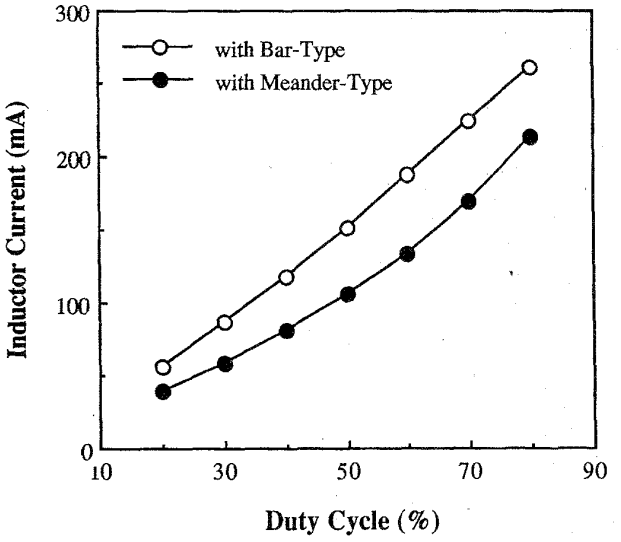

Fig. 13. Current flowing through the inductors as the function of duty cycle.

micromachined inductors is fairly low so far. However, this work is just an initial report to test a feasibility of fully integrated dc/dc power converters using micromachined inductors. The efficiency will be basically influenced from conductor resistances, magnetic properties of core materials, inductor geometries, and operating frequencies. Thus, there are still a lot of room to improve the efficiency of the integrated dc/dc converter, using new micromaching techniques to fabricate a thick high aspect ratio conductors as well as adopting new magnetic film-type materials with high operating frequencies and permeability.

As reported in [5] and [17], the permalloy core used in this study shows saturation above 0.8 Tesla. Thus, it is understandable from Fig. 12 that output voltages with the bar- and meander-type start to saturate above duty cycles of 50 and 70%, respectively. Above a duty cycle of 50%, the achievable output voltage with the meander-type inductor is higher than that with the bar-type inductor due to this magnetic flux saturation in the cores [17]. Since the output voltage can be continuously controlled as the duty cycle is adjusted, this integration feasible dc/dc boost converter has a high application potential for low voltage and micropower sources in an integrated fashion.

V. Conclusion

In this study, two planar integrated inductive components, a bar-type and a meander-type, are realized using micromachining and multilevel metal fabrication techniques. These components are suitable for magnetic micropower applications including miniaturized dc/dc converters. By using these two realized inductors, switched dc/dc boost converters are demonstrated in hybrid fashion.

In the bar-type inductor, an inductor size of 4 mm $\times$ 1.0 mm $\times$ 110 μm thickness having 33 turns of multilevel coils is realized, with an achieved specific inductance of approximately 30 nH/mm^2 at 1 MHz. In the meander-type

inductor, an inductor size of 4 mm × 1.0 mm × 130 μm thickness having 30 turns of multilevel cores is realized, with an achieved specific inductance of 35 nH/mm^2 at 1 MHz. The fabrication sequence of these inductors is entirely compatible with post-processing of standard bipolar and CMOS circuitry, as well as the fabrication of multichip module substrates, thus enabling the integration of the inductor structure with control circuitry for applications such as filters, sensors, magnetic microactuators, and low-power voltage converters.

The inductors were evaluated in a prototype switched dc/dc boost converter. The obtained maximum output voltage is approximately double an input voltage of 3 V at a switching frequency of 300 kHz and a duty cycle of 50%, demonstrating the usefulness of these integrated planar inductors. The performances of dc/dc boost converters using both inductors are also compared. The feasibility of an integrated switched dc/dc converter using the micromachined inductive components has been demonstrated in this study. As the inductor realized in this research can potentially be integrated onto a chip or module, full dc/dc converter integration can be envisaged.

ACKNOWLEDGMENT

The authors would like to gratefully acknowledge DuPont and OCG Microelectronic Materials for their donations of polyimide and Lake Shore Cryotronics, Inc. for their assistance in measurements of the magnetic properties of the permalloy thin films. Technical discussions with Prof. D. Taylor of Georgia Tech are also gratefully acknowledged. Fabrication described in this paper was performed in the Microelectronics Research Center of the Georgia Institute of Technology.

REFERENCES

[1] L. S. Fan, Y. C. Tai, and R. S. Muller, "IC-processed electrostatic micromotors," *Sensors and Actuators*, vol. 20, pp. 41–47, 1989.
[2] C. H. Ahn, Y. J. Kim, and M. G. Allen, "A fully integrated micromachined toroidal inductor with a nickel-iron magnetic core (the switched DC/DC boost converter application)," in *Proc. 7th Int. Conf. Solid-State Sensors and Actuators*, Yokohama, Japan, June 7–10, 1993, pp. 70–73.
[3] C. H. Ahn and M. G. Allen, "A comparison of two micromachined inductors for fully integrated boost DC/DC power converters," in *Proc. IEEE Applied Power Electronics Conf. (APEC)*, Orlando, FL, Feb. 1994, pp. 10–16.
[4] A. F. Goldberg, J. G. Kassakian, and M. F. Schlecht, "Issues related to 1–10 MHz transformer design," *IEEE Trans. Power Electron.*, vol. 4, pp. 113–123, 1989.
[5] C. H. Ahn, "Micromachined components as integrated inductors and magnetic microactuators," Ph.D. dissertation, Georgia Institute of Technology, Atlanta, GA, USA, 1993.
[6] I. W. Wolf, "Electrodeposition of magnetic materials," *J. Appl. Phys.*, vol. 33, no. 3, pp. 1152–1159, 1962.
[7] J. R. Corkhill and M. J. Martin, "Thick film filter designed for television signals," *Electron. Eng.*, pp. 65–69, May 1971.
[8] P. G. Barnwell, "Thick film inductors and their use in tuned circuits at VHF," *Electron. Components*, pp. 749–754, July 1971.
[9] R. F. Soohoo, "Magnetic thin film inductor for integrated circuit application," *IEEE Trans. Magn.*, vol. MAG-15, pp. 1803–1805, 1979.
[10] C. H. Ahn, Y. J. Kim, and M. G. Allen, "A fully integrated planar toroidal inductor with a micromachined nickel-iron magnetic bar," *IEEE Trans. Comp., Packag., Manufact. Technol., Part A*, vol. 17, no. 3, pp. 356–403, 1993.
[11] K. K. Chakravorty, C. P. Chien, J. M. Cech, M. H. Tanielian, and P. L. Young, "High-density interconnection using photosensitive polyimide and electroplated copper conductor lines," *IEEE Trans. Comp. Hybrids, Manufact. Technol.*, vol. 13, no. 1, pp. 200–206, 1990.
[12] C. H. Ahn and M. G. Allen, "A new toroidal-meander type integrated inductor with a multilevel meander magnetic core," *IEEE Trans. Magn.*, vol. 30, no. 1, pp. 73–79, 1994.
[13] ——, "A fully integrated surface micromachined magnetic microactuator with a multilevel meander magnetic core," *J. Microelectromech. Syst.*, vol. 2, no. 1, pp. 15–22, 1993.
[14] C. W. T. McLyman, *Transformer and Inductor Design Handbook*. New York: Marcel Dekker, 1988, pp. 84–89.
[15] R. P. Severns and G. Bloom, *Modern DC/DC Switchmode Power Converter Circuits*. New York: Van Nostrand, 1985, pp. 61–77.
[16] T. Ninomiya, K. Harada, and M. Nakahara, "On the maximum regulation range in boost and buck-boost converters," in *Proc. IEEE PESC*, 1981, pp. 146–153.
[17] C. H. Ahn and M. G. Allen, "A planar micromachined spiral inductor for magnetic microactuator applications," *J. Micromechanics and Microengineering*, vol. 3, no. 3, pp. 1–9, 1993.

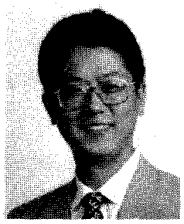

Chong H. Ahn (M'92) received the B.S. degree in electrical engineering from Inha University, Korea, in 1980, the M.S. degree in electrical engineering from the Seoul National University, Korea, in 1983, and the Ph.D. degree in electrical and computer engineering from the Georgia Institute of Technology in 1993.

He worked as a Post-Doctoral Fellow at IBM Thomas J. Watson Research Center, and then he joined the University of Cincinnati, where he is currently Assistant Professor in the Department of Electrical and Computer Engineering and Computer Science. His research interests include microelectromechanical systems (MEMS), microsensors and microactuators, micromachined magnetic components, and micro-power electronics.

Dr. Ahn is a member of ASME.

Mark G. Allen (M'89) received the B.A. degree in chemistry, the B.S.E. degree in chemical engineering, and the B.S.E. degree in electrical engineering from the University of Pennsylvania in 1984, the S.M. degree from the Massachusetts Institute of Technology (M.I.T.) in 1986, and the Ph.D. degree from M.I.T. in 1989.

In 1989 he joined the Georgia Institute of Technology, where he is currently Associate Professor of Electrical and Computer Engineering. His research include micromaching fabrication technology, micro-optomechanical systems, and material issues in micromachined structures and electronic packages.

Dr. Allen is a member of the editorial board of the *Journal of Micromechanics and Microengineering*.